Luminescence Behavior of Sol−Gel-Derived Hybrid Materials Resulting from Covalent Grafting of a Chromophore Unit to Different Organically Modified Alkoxysilanes

Anne-Christine Franville, Daniel Zambon,* and Rachid Mahiou

Laboratoire des Matériaux Inorganiques, UPRES-A CNRS 6002, Université Blaise Pascal, 63177 Aubière Cedex, France

Yves Troin

Laboratoire de Chimie des Hétérocycles et des Glucides, EA 987, Ecole Nationale Supérieure de Chimie de Clermont-Ferrand, 63174 Aubière Cedex, France

Received July 27, 1999

The compounds studied in this work are sol−gel-derived organic−inorganic hybrid materials in which the two components are covalently linked via Si−C bonds. The organic part is a chromophore group derived from dipicolinic acid that is functionalized with trialkoxysilyl groups; the as-obtained silylated monomers are afterward submitted to complexation with rare-earth ions (Eu^{3+}, Gd^{3+}) and are used as the siloxane network precursors. The preparation of hybrid materials including covalent grafting and the sol−gel process is described, as well as their luminescence properties. Modifications of the ligand structure (mono- or disubstituted amides) lead to different coordinating properties and to variable absorption edges. As a result, the absorption efficiency or the ability of the chelates to transfer the absorbed energy to Ln^{3+} and consequently the quantum yield of the emission are changed. The major effect of silica is a broadening of the emission peaks, whereas spectral repartitions and lifetimes are mainly unchanged as compared with the corresponding organic molecules.

1. Introduction

Organic−inorganic hybrid materials have been widely studied in the past decade because these systems exhibit unique properties in many fields of applications as they combine the respective characteristics of organic and inorganic parts.[1−2] The sol−gel technique has proven to be a convenient route for the preparation of such hybrid compounds.[3−4] This method consists of an inorganic polymerization based on hydrolysis/condensation reactions of metal alkoxides.[5−6] The low-temperature processing allows the incorporation of organic moieties into an inorganic network, and the use of molecular precursors leads to composite materials on a nanometer scale. The versatility of the method is another tremendous advantage; the very large choice for the two components offers the opportunity to obtain materials with various compositions and therefore with flexible properties. These properties can be further tailored by modifying the sol−gel processing conditions that allow, for example, for the control of the microstructure, the shape, and the degree of connection between the two networks.[7−9]

Sol−gel-derived siloxane hybrid materials have attracted much interest for photonic applications as they potentially combine the optical quality of silica, its thermal stability, and its mechanical strength, together with the optical characteristics of active organic molecules.[10−12] This approach seems to be suitable for the design of highly luminescent materials. Indeed, rare-earth organic complexes embedded in silica gels have been shown to exhibit improved emission properties with respect to simple metal ions in similar matrixes.[13] Organic chelates are known to be efficient sensitizers for the luminescence of lanthanide ions (Eu^{3+} and Tb^{3+} in particular), the so-called antenna effect.[14] They also reduce both the concentration and the OH quenchings, which have shown to be very important in siloxane matrixes.[15−17] Entrapping of rare-earth complexes with

(1) Wen, J.; Wilkes, G. L. *Chem. Mater.* **1996**, *8* (8), 1667.
(2) Sanchez, C.; Babonneau, F. *Matériaux Hybrides*; Observatoire Français des Techniques Avancées, Masson: Paris, 1996.
(3) Sanchez, C.; Ribot, F. *New J. Chem.* **1994**, *18* (10), 1007.
(4) Corriu, R.; Leclercq, D. *Angew. Chem., Int. Ed. Engl.* **1996**, *35*, 1420.
(5) Hench, L. L.; West, J. K. *Chem. Rev.* **1990**, *90*, (1), 33.
(6) Brinker, C. J.; Sherrer, G. W. *Sol−Gel Science*; Academic Press: Boston, 1990.
(7) Corriu, R. *C. R. Acad. Sci. Paris* **1998**, *1*, Série IIc, 83.
(8) Judeinstein, P.; Sanchez, C. *J. Mater. Chem.* **1996**, *6* (4), 511.
(9) Schubert, U. *J. Chem. Soc., Dalton Trans.* **1996**, *16*, 3343.
(10) Seddon, A. B. *I. E. E. Proc. Circuits Devices Syst.* **1998**, *145* (4), 369.
(11) Pope, E. J. A. *J. Sol-Gel Sci. Technol.* **1994**, *2*, 717.
(12) Boilot, J. P.; Chaput, F.; Gacoin, T.; Malier, L.; Canva, M.; Brun, A.; Lévy, Y.; Galaup, J. P. *C. R. Acad. Sci. Paris* **1996**, *322*, Série IIb, 27.
(13) Matthews, L. R.; Knobbe, E. T. *Chem. Mater.* **1993**, *5* (12), 1697.
(14) Sabbatini, N.; Guardigli, M.; Lehn, J. M. *Coord. Chem. Rev.* **1993**, *123*, 201.
(15) Viana, B.; Koslova, N.; Aschehoug, P.; Sanchez, C. *J. Mater. Chem.* **1995**, *5*, 719.

10.1021/cm9904739 CCC: $19.00
Published on Web 01/04/2000

β-diketones, aromatic carboxylic acids, and heterocyclic ligands in sol−gel-derived host structures has been described in some recent studies.[13,18−23] Typically, these materials were obtained by doping silica gels with organometallic complexes (class I hybrid materials[3]). Clustering of emitting species is however difficult to prevent by this method as only weak interactions (typically hydrogen bonds or van der Waals forces) exist between organic and inorganic parts. Inhomogeneous dispersion of both components and leaching of dopants are observed in class I hybrid materials for which the concentration of organic species is also limited. In this study, covalent grafting of the ligand to the silica backbone via Si−C bonds will allow us to overcome these drawbacks. The as-derived class II[3] hybrid organic−inorganic luminescent materials were monophasic even at a high concentration of organic chelates, and the reinforcement of thermal and mechanical resistances has been clearly established.[24]

In this paper, the synthesis and characterizations of silylated ligands derived from dipicolinic acid are described; the derived multifunctional organosilanes were afterward submitted to complexation with Eu^{3+}/Gd^{3+} ions and to a sol−gel process in order to obtain the hybrid materials. Silica precursors are grafted to the chromophore via amide linkages, and different substituents (alkyl chains or phenyl groups) were introduced on the N atom of the amide bond. In this way, subsequent modifications in the local environment of Eu^{3+} are expected to change the luminescence characteristics of the metal ion. Indeed, N−H groups are likely to induce nonradiative decay mechanisms in a manner similar to that of O−H oscillators (ν(NH) = 3300 cm^{-1} and ν(OH) = 3400 cm^{-1}),[25−27] and additional aromatic groups can moreover improve the absorption efficiency. Optical spectra of the hybrid materials will be discussed in relation to the ligand structure and compared with those of the corresponding organic complexes.

2. Experimental Section

Starting Materials and Experimental Techniques. Starting materials were purchased from Aldrich or Fluka and were used as received except organic amines (*N*-butylamine, *N*-methylbutylamine, dibutylamine, and *N*-butylaniline) and pyridine, which were dried over KOH and distilled in the presence of BaO. All solvents were distilled before utilization according to the literature procedures.[28] Europium and gadolinium nitrates were obtained from the corresponding oxides in dilute nitric acid.

Scheme 1. Synthesis of Silylated Ligands and Their Organic Analogues via Amidation[a]

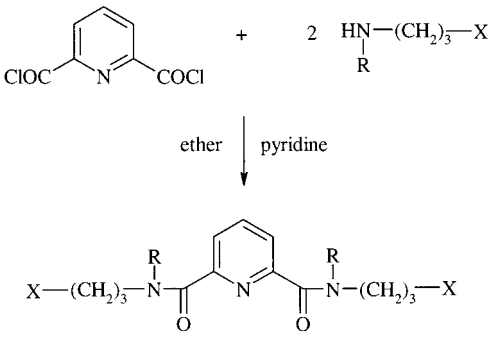

[a] Significance of R and X is given in Scheme 2.

^{1}H and ^{13}C NMR spectra were recorded on a Bruker AC 400 spectrometer with tetramethylsilane as an internal reference. In the following sections, the abbreviations used are s for singlet, bs for broad singlet, d for doublet, t for triplet, q for quadruplet, and m for multiplet. Infrared absorption spectra were obtained as KBr pellets or neat on a Nicolet model 5SXC FT-IR spectrometer. Electron impact (EI) mass spectra were recorded on a Hewlett-Packard 5989B spectrometer (70 eV). Fast atom bombardment (FAB) mass measurements were performed at CRMPO (Université de Rennes, France) with a Varian Mat 311 spectrometer, and elemental analyses were performed by the Service Central d'Analyse (CNRS, France). Reflectivity spectra were recorded on a Perkin-Elmer Lambda 2S spectrometer equipped with a diffuse reflectance accessory. Luminescence measurements were performed at low temperature (15 K). Sample cooling was provided by closed cycle He optical cryostat (Cryomech GB-15). Emission spectra were obtained using either the 337.1 nm radiation supplied by a pulsed nitrogen laser (Jobin-Yvon LA04) or the 290 nm radiation extracted by appropriate filters from the KDP-doubled laser beam delivered by a ND60 continuum dye laser working with a mixture of Rh590 and Rh610 in solution. Excitation spectra were recorded using a Xe lamp, and luminescence lifetime measurements were made using a Lecroy 9310A-400 MHz oscilloscope.

Synthesis of the Ligands. Silylated monomers and their organic analogues were prepared according to the procedure depicted in Scheme 1, using 2,6-pyridinedicarboxylic acid chloride (dipicolinic acid chloride) as starting reagent. The respective formulas of the derived ligands are shown in Scheme 2. The coupling reaction was performed by addition of acid chloride functions on primary or secondary amino alkyl silanes, therefore establishing double amide linkage between the silica precursor and the chromophore. The structure of the organic ligands was identical to that of the silylated derivatives with methyl groups instead of trialkoxysilyl functions.

Synthesis of the Silylated Monomers. Silylated monomer S_1 was prepared as follows: 0.5000 g (2.45 mmol) of 2,6-pyridinedicarboxylic acid chloride was dissolved in 50 mL of dry diethyl ether and degassed under argon. A solution of (3-aminopropyl)triethoxysilane (1.0850 g, 4.90 mmol) and pyridine (0.4260 g, 5.39 mmol) in 20 mL of diethyl ether was then added dropwise to the mixture. The resulting solution was stirred under argon for 4 h at room temperature. Filtration of the precipitated pyridinium hydrochloride followed by evaporation of diethyl ether and excess pyridine led to a residue that was further dried on a vacuum line, furnishing ligand S_1 as a clear oil (1.36 g) in a 97% yield.

S_1 (yellow oil): ^{1}H NMR ($CDCl_3$, 400 MHz) δ (ppm) 8.30 (d, J = 7.5 Hz, 2H, H_3−H_5), 8.15 (bs, 2H, NH), 8.02 (t, J = 7.5

(16) Campostrini, R.; Ferrari, M.; Montagna, M.; Pilla, O. *J. Mater. Res.* **1992**, *7*, 745.
(17) Lochhead, M.; Bray, K. L. *Chem. Mater.* **1995**, *7* (4), 572.
(18) Yan, B.; Zhang, H. J.; Ni, J. Z. *Mater. Sci. Eng.* **1998**, *B52*, 123.
(19) Serra, O. A.; Nassar, E. I.; Zapparolli, G.; Rosa, I. L. V. *J. Alloys Compd.* **1994**, *207/208*, 454.
(20) Zhang, Y.; Wang, M.; Xu, J. *J. Mater. Sci. Eng.* **1997**, *B47*, 23.
(21) Serra, O. A.; Nassar, E. J.; Rosa, I. L. V. *J. Lumin.* **1997**, *72−74*, 263.
(22) Czarnobaj, K.; Elbanowski, M.; Hnatejko, Z.; Klonkowski, A. M.; Lis, M.; Pietraszkiewicz, M. *Spectrochim. Acta, Part A* **1998**, *54*, 2183.
(23) Bredol, M.; Kynast, U.; Boldhaus, M.; Lau, C. *Ber. Bunsen-Ges. Phys. Chem.* **1998**, *102* (11), 1557.
(24) Franville, A. C.; Zambon, D.; Mahiou, R.; Chou, S.; Troin, Y.; Cousseins, J. C. *J. Alloys Compd.* **1998**, *275−277*, 831.
(25) Wang, Z.; Choppin, G. R.; Di Bernardo, P.; Zanonato, P. L.; Portanova, R.; Tolazzi, M. *J. Chem. Soc., Dalton Trans.* **1993**, 2791.
(26) Dickins, R. S.; Parker, D.; De Sousa, A. S.; Williams, J. A. G. *Chem. Commun.* **1996**, 697.
(27) Beeby, A.; Clarkson, I. M.; Dickins, R. S.; Faulkner, S.; Parker, D.; Royle, L.; De Sousa, A. S.; Williams, J. A. G.; Woods, M. *J. Chem. Soc., Perkin Trans. 2* **1999**, *3*, 493.
(28) Perrin, D. D.; Armarego, W. L. F.; Perrin, D. R. *Purification of Laboratory Chemicals*, 2nd ed.; Pergamon Press: Oxford, 1980.

Scheme 2. Structure of the Silylated Monomers and of the Organic Ligands[a]

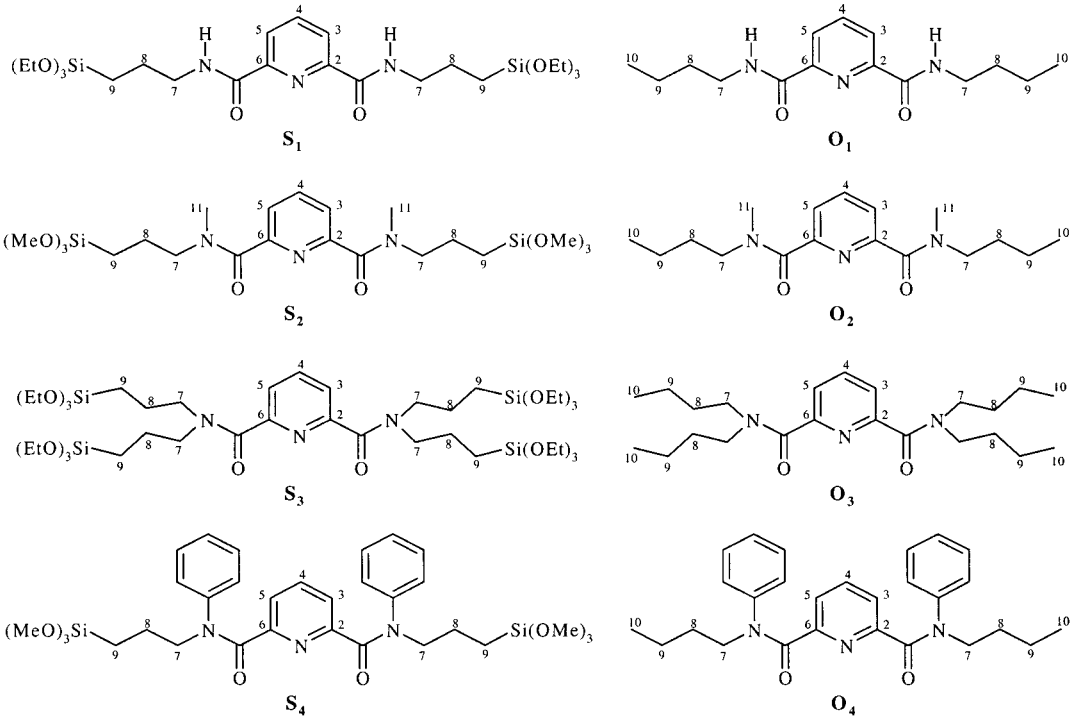

[a] Carbon numbering is shown on the scheme.

Hz, 1H, H_4), 3.82 (q, $J = 6.2$ Hz, 12H, CH_2(OEt)), 3.50 (t, $J = 6.7$ Hz, 4H, H_7), 1.80 (quint, $J = 6.7$ Hz, 4H, H_8), 1.22 (t, $J = 6.2$ Hz, 18H, CH_3(OEt)), 0.72 (t, $J = 6.7$ Hz, 4H, H_9); ^{13}C NMR ($CDCl_3$, 100 MHz) δ (ppm) 163.6 (C═O), 149.0 (C_2-C_6), 138.9 (C_3-C_5), 124.9 (C_4), 58.5 (CH_2(OEt)), 42.0 (C_7), 23.2 (C_8), 18.3 (CH_3(OEt)), 7.9 (C_9); MS (EI) $m/e = 573$ (M^+).

Silylated monomers S_2-S_4 were prepared as previously described for ligand S_1 starting from [3-(methylamino)propyl]-trimethoxysilane, bis[3(triethoxysilyl)propyl]amine, and *N*-[3-(trimethoxysilyl)propyl]aniline, respectively.

S_2 (yellow oil): ^{1}H NMR ($CDCl_3$, 400 MHz) δ (ppm) 7.93 (t, $J = 7.9$ Hz, 1H, H_4), 7.68 (d, $J = 7.9$ Hz, 2H, H_3-H_5), 3.60−3.50 (s, 18H, CH_3(OMe)), 3.55−3.33 (t, $J = 7.0$ Hz, 4H, H_7), 3.10−3.02 (s, 6H, H_{11}), 1.80−1.70 (m, 4H, H_8), 0.73−0.45 (t, $J = 7.0$ Hz, 4H, H_9); ^{13}C NMR ($CDCl_3$, 100 MHz) δ (ppm) 168.5−167.9 (C═O), 153.3−153.2 (C_2-C_6), 137.9 (C_3-C_5), 124.0 (C_4), 50.8 (CH_3(OMe)), 53.3−50.5 (C_7), 36.9−33.2 (C_{11}), 21.5−20.0 (C_8), 6.3−5.8 (C_9); MS (EI) $m/e = 517$ (M^+).

S_3 (yellow oil): ^{1}H NMR ($CDCl_3$, 400 MHz) δ (ppm) 7.84 (t, $J = 8.5$ Hz, 1H, H_4), 7.54 (d, $J = 8.5$ Hz, 2H, H_3-H_5), 3.82−3.75 (q, $J = 6.2$ Hz, 24H, CH_2(OEt)), 3.47−3.30 (t, $J = 7.3$ Hz, 8H, H_7), 1.78−1.60 (m, 8H, H_8), 1.22−1.17 (t, $J = 6.2$ Hz, 36H, CH_3(OEt)), 0.67−0.35 (t, $J = 7.3$ Hz, 8H, H_9); ^{13}C NMR ($CDCl_3$, 100 MHz) δ (ppm) 168.3 (C═O), 153.9 (C_2-C_6), 137.8 (C_3-C_5), 123.5 (C_4), 58.4 (CH_2(OEt)), 51.2−48.5 (C_7), 22.4−20.9 (C_8), 18.4 (CH_3(OEt)), 7.9−7.3 (C_9); MS (EI) $m/e = 982$ $(M + H)^+$.

S_4 (orange oil): ^{1}H NMR ($CDCl_3$, 400 MHz) δ (ppm) 7.15 (bs, 10H, H_{aro}), 6.82 (bs, 3H, H_{aro}), 3.82 (bs, 4H, H_7), 3.50 (bs, 18H, CH_3(OMe)), 1.67 (bs, 4H, H_8), 0.65 (bs, 4H, H_9); ^{13}C NMR ($CDCl_3$, 100 MHz) δ (ppm) 167.4 (C═O), 153.0 (C_2-C_6), 142.7 (C_{aro}), 135.9 (C_3-C_5), 128.8−127.8−126.7 (CH_{aro}), 123.5 (C_4), 52.3 (C_7), 50.5 (CH_3(OMe)), 20.6 (C_8), 6.3 (C_9); MS (EI) $m/e = 641$ (M^+).

Synthesis of the Organic Ligands. The procedure used for the silylated monomers was slightly modified for the synthesis of the organic ligands in the following manner. A typical procedure is given below for ligand O_1. 2,6-Pyridinedicarboxylic acid chloride (0.5000 g, 2.45 mmol) and 0.3598 g (4.90 mmol) of *N*-butylamine were reacted under argon for 3 h at room temperature in the presence of excess pyridine and using diethyl ether as a solvent. Pyridinium hydrochloride was filtered, and residual organic solvents were eliminated by evaporation. The resulting solid was dissolved in dichloromethane, washed with aqueous 5% $NaHCO_3$, and dried over Na_2SO_4. Evaporation of the solvent gave the amide O_1 with a good yield (95%). Analytical sample was obtained by flash chromatography on silica gel.

O_1 (white solid): mp 154 °C; ^{1}H NMR ($CDCl_3$, 400 MHz) δ (ppm) 8.35 (d, $J = 7.6$ Hz, 2H, H_3-H_5), 8.05 (t, $J = 7.6$ Hz, 1H, H_4), 7.75 (bs, 2H, NH), 3.50 (t, $J = 6.0$ Hz, 4H, H_7), 1.65 (quint, $J = 6.0$ Hz, 4H, H_8), 1.42 (m, 4H, H_9), 1.00 (t, $J = 6.0$ Hz, 6H, H_{10}); ^{13}C NMR ($CDCl_3$, 100 MHz) δ (ppm) 163.7 (C═O), 149.0 (C_2-C_6), 139.0 (C_3-C_5), 124.9 (C_4), 39.4 (C_7), 31.8 (C_8), 20.2 (C_9), 13.8 (C_{10}); MS (EI) $m/e = 277$ (M^+). Anal. for $C_{15}H_{23}N_3O_2$: found, C 65.06, H 8.33, N 15.27; calcd C 64.95, H 8.36, N 15.15.

Ligands O_2-O_4 were prepared following the same procedure as above from *N*-methylbutylamine, dibutylamine, and *N*-butylaniline, respectively.

O_2 (orange oil): ^{1}H NMR ($CDCl_3$, 400 MHz) δ (ppm) 7.85 (t, $J = 10.5$ Hz, 1H, H_4), 7.57 (d, $J = 10.5$ Hz, 2H, H_3-H_5), 3.45−3.25 (t, $J = 7.9$ Hz, 4H, H_7), 3.05−2.95 (s, 6H, H_{11}), 1.67−1.47 (m, 4H, H_8), 1.35−1.10 (m, 4H, H_9), 0.93−0.75 (t, $J = 7.9$ Hz, 6H, H_{10}); ^{13}C NMR ($CDCl_3$, 100 MHz) δ (ppm) 168.4−168.0 (C═O), 153.3−153.2 (C_2-C_6), 138.0 (C_3-C_5), 123.9 (C_4), 50.7−47.8 (C_7), 37.0−33.4 (C_{11}), 30.4−29.0 (C_8), 20.1−19.6 (C_9), 13.9−13.7 (C_{10}); HRMS (FAB) $[M + H]^+$ found 306.2198, calculated for $C_{17}H_{27}N_3O_2$ 306.2182.

O_3 (colorless oil): ^{1}H NMR ($CDCl_3$, 400 MHz) δ (ppm) 7.85 (t, $J = 7.5$ Hz, 1H, H_4), 7.57 (d, $J = 7.5$ Hz, 2H, H_3-H_5), 3.45−3.23 (t, $J = 6.5$ Hz, 8H, H_7), 1.65−1.50 (quint, $J = 6.5$ Hz, 8H, H_8), 1.37−1.12 (m, 8H, H_9), 0.98−0.80 (t, $J = 6.5$ Hz, 12H, H_{10}); ^{13}C NMR ($CDCl_3$, 100 MHz) δ (ppm) 168.2 (C═O), 153.6 (C_2-C_6), 137.9 (C_3-C_5), 123.9 (C_4), 48.6−45.6 (C_7), 31.0−29.6 (C_8), 20.3−19.8 (C_9), 14.0−13.8 (C_{10}); HRMS (FAB) $[M + H]^+$ found 390.3125, calcd for $C_{23}H_{39}N_3O_2$ 390.3121.

O_4 (white solid): mp 130 °C; ^{1}H NMR ($CDCl_3$, 400 MHz) δ (ppm) 7.35 (bs, 1H, H_4), 7.20 (bs, 10H, H_{aro}), 6.80 (bs, 2H, H_3-H_5), 3.85 (bs, 4H, H_7), 1.55 (bs, 4H, H_8), 1.35 (bs, 4H, H_9), 0.90 (bs, 6H, H_{10}); ^{13}C NMR ($CDCl_3$, 100 MHz) δ (ppm) 167.5 (C═O), 153.2 (C_2-C_6), 142.9 (C_{aro}), 136.1 (C_3-C_5), 128.8−128.0−126.8 (CH_{aro}), 123.7 (C_4), 49.9 (C_7), 29.7 (C_8), 20.1 (C_9), 13.9 (C_{10}); MS (EI) $m/e = 641$ (M^+). Anal. for $C_{27}H_{31}N_3O_2$: found, C 75.53, H 7.23, N 9.80; calcd, C 75.49, H 7.27, N 9.78.

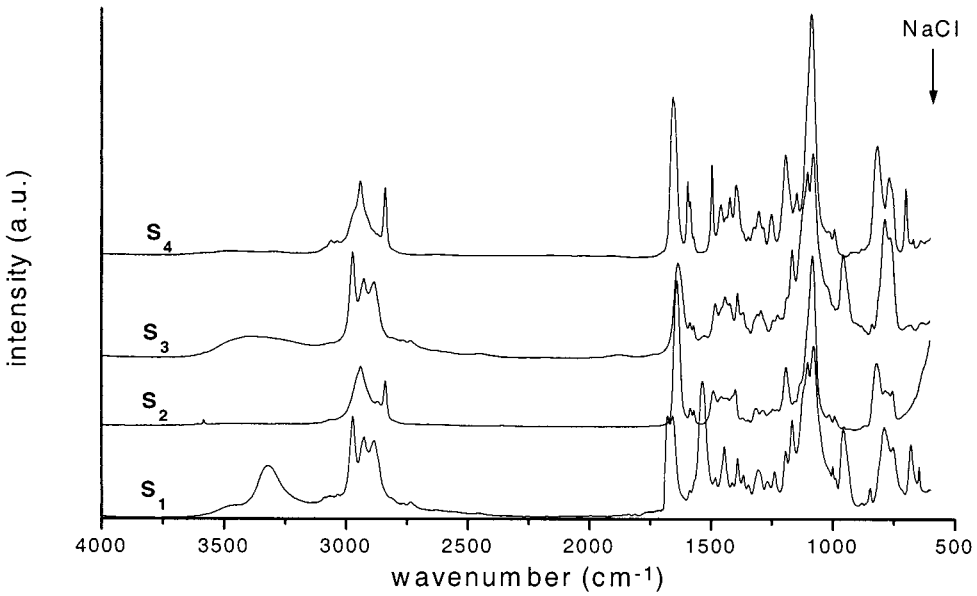

Figure 1. Infrared spectra of silylated ligands in the 4000−500 cm^{-1} range.

Synthesis of the Hybrid Complexes and Their Organic Analogues. *Synthesis of Hybrid Complexes from Silylated Monomers.* Silylated monomers were used as the only siloxane network precursors. The sol−gel syntheses were carried out in an ethanolic (for S_1-S_3) or methanolic (for S_2-S_4) medium. Complexation with Eu^{3+} and Gd^{3+} ions was performed in the same solvent, with the Ln^{3+} ions being introduced as nitrate salts ($Eu(NO_3)_3$, $6H_2O$, and $Gd(NO_3)_3$, $6H_2O$, respectively). The Ln^{3+}/S_j ($j = 1-4$) molar ratio was taken as $^1/_3$, and the H_2O/Si molar ratio was $^1/_1$. Because lanthanide nitrates are obtained as hexahydrates, they provide the required moles of water except for ligand S_3. In this case, additional water was introduced to obtain the same H_2O/Si equimolar ratio. In a typical sol preparation, the silylated monomer was dissolved in absolute alcohol, and appropriate amounts of europium (gadolinium) nitrate in solution were then added. The mixture was vigorously stirred for 1 h before introducing hydrochloric acid to promote hydrolysis (pH = 2). The amount of HCl was considered to be negligible and thus does not change the H_2O/Si molar ratio. The solution was stirred for 30 additional min, and the resulting sol was aged in covered Teflon beakers at room temperature until the onset of gelation, which occurred within 8−10 days. The gels were obtained as monolithic bulks that were ground for the luminescence studies. The obtained powder materials were washed with ethanol or methanol and dried at 70 °C for 2 days. The resulting hybrid compounds are afterward noted EuS_j and GdS_j, with $j = 1-4$.

Synthesis of Complexes from Organic Ligands. Europium and gadolinium complexes with ligands O_1-O_4 were prepared by addition of a solution of the corresponding lanthanide nitrate in dry acetonitrile to the ligand previously dissolved in the same solvent with a $^1/_3$ Ln^{3+}/ligand stoichiometric ratio. The resulting mixture was heated under reflux for 2 h. In the case of ligand O_1, a white solid precipitated after cooling. This precipitate was filtered, washed several times with acetonitrile, and dried. Complexes with ligands O_3-O_4 were precipitated by slow addition of diethyl ether after removal of the solvent by evaporation and then were isolated by filtration, washed with ether, and dried in a vacuum desiccator overnight. The as-synthesized compounds are later denoted as EuO_j and GdO_j, with $j = 1-4$. Europium complex with ligand O_2 could not be obtained as solid powder and was isolated as an orange oil whose optical properties could not be investigated using the experimental techniques aforementioned.

3. Results and Discussion

Chemical Characterizations. *Free Ligands Characterizations.* As detailed in the Experimental Section, ^1H and ^{13}C NMR spectra as well as mass spectra relative to the silylated ligands are in full agreement with the proposed structures. Integration of the ^1H NMR signals corresponding to ethoxy or methoxy groups shows that no hydrolysis of the precursors occurred during the grafting reaction. The single peak observed for carbonyl groups in ^{13}C NMR spectra is attributed to the amide function and demonstrates that the whole amount of 2,6-pyridinedicarboxylic acid chloride has reacted. The ^{13}C NMR chemical shifts relative to C═O bonds are identical for silylated and organic ligands and are indicative of the amide substitution degree (164 ppm for monosubstituted species and 168 ppm for disubstituted ones). Splitting of the NMR signals for O_2/S_2 and O_3/S_3 ligands indicates that free rotation about the C−N bond is prevented by substitution groups as commonly observed for disubstituted amides. When considering phenyl substituents, this rotation is fully hindered, which leads to coalescence.

FTIR experiments were performed on silylated and organic ligands. IR spectra of S_1-S_4 ligands are presented in Figure 1, and assignments of the vibration frequencies for all ligands are given in Table 1. The spectra relative to silylated ligands are dominated by the ν(Si−C) and ν(Si−OEt) (or ν(Si−OMe)) absorption bands characteristic of trialkoxysilyl functions. The grafting reaction is evidenced by the sharp band located at 1680−1640 cm^{-1}, corresponding to amide groups. No absorption band characteristic of carboxylic acid chloride or carboxylic acid functions was detected in the range 1760−1720 cm^{-1}, which is a further proof of the completion of reaction. Splitting of the ν(C═O) vibration mode observed for O_1 and S_1 ligands arises from the coexistence of trans and cis conformations, whereas other ligands are only in the trans form. The stretching ν(NH) and bending δ(NH) vibration modes located near 3320 and 1535 cm^{-1}, respectively, are also clearly evidenced in IR spectra of monosubstituted amides (ligands O_1 and S_1). Changing secondary amide functions to tertiary ones (ligands S_j/O_j, with $j = 2-4$) induces disappearance of these absorption bands together with shifts to lower frequencies of the ν(C═O) stretching vibration. Indeed,

Table 1. Assignments of the Infrared Absorption Bands in the 4000−1000 cm^{-1} Range for Silylated Monomers and Organic Ligands

	S_1	O_1	S_2	O_2	S_3	O_3	S_4	O_4
ν(NH)	3322	3327−3277						
aromatic	3070	3069	3065	3065		3068	3062	3054
$\nu_{as}(CH_3)$	2973	2959		2957	2973	2958		2953
$\nu_{as}(CH_2)$	2927	2931	2941	2932	2927	2932	2942	2932
$\nu_s(CH_3-CH_2)$	2885	2868	2872−2840	2872	2886	2872	2840	2869
ν(C=O)	1678−1657	1679−1652	1640	1640	1635	1636	1655	1660
aromatic	1587	1590	1585−1570	1584−1570	1586−1571	1586−1567	1595−1585	1597−1577
δ(NH)-ν(CN)	1535	1541						
aromatic	1481	1460	1490−1457	1492−1458	1481	1479−1460	1495−1458	1496−1457
$\delta_{as}(CH_3)$	1445	1443	1443	1432	1442	1435		
$\delta(CH_2)$	1412	1413	1400	1400	1421	1420	1422	1421
$\delta_s(CH_3)$	1390	1373		1379	1390	1383	1396	1396
$\delta(CH_2)$	1366−1346		1370−1347		1367		1346	
ν(C−C)	1306	1310	1314−1287	1311	1307−1294	1315	1303	1305
$(CH_2)_{wag}$	1268−1238	1243−1221	1246−1229	1259−1228	1244−1225	1251−1228	1251	1252
δ(C−C)$_{skel}$		1173−1144−1073		1191−1155−1115−1077		1189−1152−1121−1082-		1196−1178−1131−1081
ν(Si−C)	1193		1192		1188		1193	
ν(Si−OEt)	1167−1103−1079−957				1167−1103−1080−957			
ν(Si−OMe)			1083−1015				1083−1017	

ν(C=O) is typically located at 1660 cm^{-1} for monosubstituted amides and at 1640 cm^{-1} for disubstituted ones. The intermediate frequency observed for ν(C=O) when phenyl groups are attached to the N atom (1655 cm^{-1}) is ascribed to the electron-withdrawing ability of the aromatic system, thus decreasing the electron density on the oxygen atom of the carbonyl group.[29] Generally speaking, decreasing ν(C=O) frequencies are related to a more ionic character of the amide bond. As derived from the values reported in Table 1, this ionic character differs according to the substituents (H, alkyl, phenyl) and the resulting coordinating properties are likely to be modified. In a similar way, no difference appears in the ν(C=O) vibration frequency between the two kinds of ligands O_j and S_j. The electron distribution within the carbonyl bond remains therefore unchanged upon addition of trialkoxysilyl groups due to the presence of $(CH_2)_n$ spacers, which allows the bond to keep the silicon atoms (electron-donating character) and amide functions apart from each other. Consequently, silylated ligands would have the same chelating ability as their organic analogues. The $(CH_2)_n$ spacers are also determining in avoiding steric hindrance from the alkoxy groups during complexation.

Hybrid and Organic Complexes Characterizations. Sol−gel process performed on silylated ligands lead to amorphous materials, which were characterized by infrared spectroscopy. The ν(Si−C) vibration located in the 1188−1193 cm^{-1} wavelength range is observed in IR spectra of hybrid materials, which is consistent with the fact that no (Si−C) bond cleavage occurs during hydrolysis/condensation reactions. The broad absorption band at 1120−1000 cm^{-1} (ν(Si−O−Si)) indicates the formation of siloxane bonds and residual silanol groups are evidenced by the ν(Si−OH) stretching vibration at 900 cm^{-1}. Condensation reactions are therefore not complete, as it is expected when using organically modified alkoxysilanes as silica network precursors.

Complexation of Ln^{3+} ions by the ligands is clearly shown by infrared spectroscopy. Indeed, ν(C=O) vibrations are shifted to lower frequencies ($\Delta\nu = 20-40$ cm^{-1}) after complexation of the metallic ion with the oxygen atom of the carbonyl group. Table 2 summarizes the ν(C=O) frequencies observed for free and coordinated ligands. In the case of monosubstituted amides (O_1−S_1), complexation also induces a shift of δ(NH) absorption bands to higher frequencies. A shoulder located near 1660−1635 cm^{-1} is noted for EuS_4/GdS_4 hybrid chelates and is attributed to the remaining free ligands. Steric hindrance from the phenyl groups probably explains the incomplete complexation reaction in that case, but the proportion of uncoordinated ligands S_4 remains however weak. As derived from the ν(C=O) frequency values relative to coordinated ligands, the $Ln^{3+}\cdots O{=}C$ bond is expected to be stronger for disubstituted amides than for monosubstituted ones. Replacing Eu^{3+} by Gd^{3+} or changing organic ligands into silylated ones seems to have no influence on the $Ln^{3+}\cdots O{=}C$ bond strength. As previously reported,[24] a 9-fold coordination involving three nitrogen atoms of pyridine units and six oxygen atoms of carbonyl groups is observed for Ln^{3+} ions, and the resulting predicted EuS_1 complex structure is presented as an example in Scheme 3. However, the presence of H_2O molecules or OH groups in the coordination sphere cannot be excluded.

Table 2. ν(C=O) Stretching Vibration Frequencies[a] for Free and Coordinated Ligands

	free ligand	Eu^{3+} complex	Gd^{3+} complex
S_1	1678−1657	1637	1638
S_2	1640	1611	1612
S_3	1635	1605	1608
S_4	1655	1611 + sh[b]	1610 + sh[b]
O_1	1679−1648	1635	1636
O_2	1640		1612
O_3	1636	1603	1602
O_4	1660	1612	1613

[a] In inverse centimeters. [b] sh = shoulder; see text for explanations.

Luminescence Properties. Amide functions are already well-known to be good chelating groups to sensitize luminescence of lanthanide complexes.[30−32] The mechanism usually described for sensitized emission in rare-earth chelates proceeds through the follow-

(29) Lin-Vien, P.; Colthup, N. B.; Fateley, W. G.; Grasselli, J. G. *The Handbook of Infrared and Raman Characteristic Frequencies of Organic Molecules*; Academic Press: San Diego, 1991.

Scheme 3. Predicted Structure of the EuS_1 Hybrid Compound

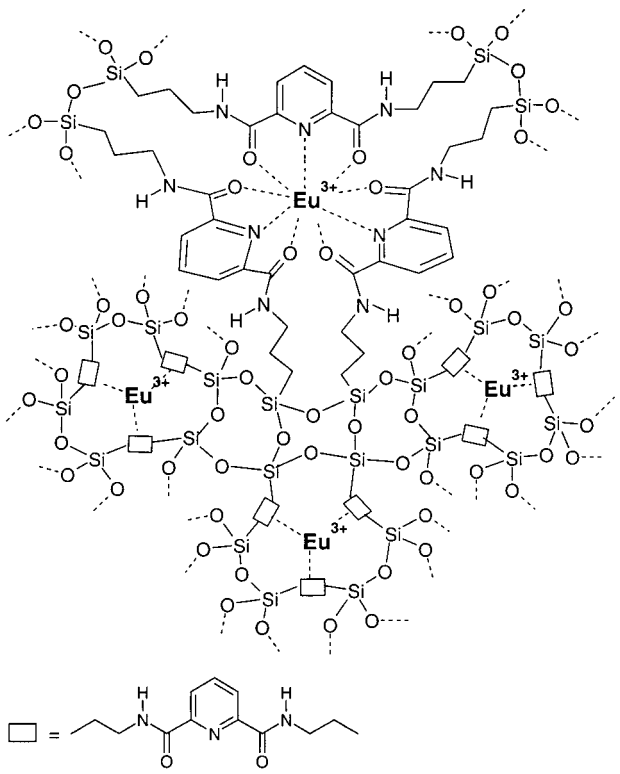

ing steps: (i) absorption via a ground singlet-excited singlet transition, (ii) radiationless intersystem crossing from the excited singlet to the triplet state, (iii) ligand-to-metal energy transfer to excited metal ion states, and (iv) emission from the Eu^{3+} $^5D_0$ excited state. This phenomenon has been reviewed by Crosby et al.[33] and energy transfer mechanisms have been extensively discussed.[34−35]

Position of the Energy Levels Relative to the Ligands. Diffuse reflectance experiments were performed on powdered materials, for both free and coordinated ligands. Reflectivity spectra exhibit for all samples a broad absorption band in the near-UV range (200−350 nm). This absorption band corresponds to transition from the ground state of the ligand to the first excited state ($S_0 \rightarrow S_1$). It is more specifically attributed to $\pi \rightarrow \pi^*$ transition in the aromatic group. The absorption edges (λ_{abs}) were extracted from the spectra and are reported in Table 3. For all ligands, a red shift is observed upon complexation. The singlet level is sensitive to the ligand structure, and the absorption edge positions (in nm) are found to decrease in the order of: $\lambda_{abs}(O_1-S_1) \leq \lambda_{abs}(O_2-S_2)-\lambda_{abs}(O_3-S_3) < \lambda_{abs}(O_4-S_4)$. In particular, the influence of phenyl groups is very sensitive. This is due to enhanced delocalization in the aromatic system. By comparison, the modifications induced by alkyl chains are less evident. In view of the

Table 3. Absorption and Excitation Maxima, Position of the Triplet State Levels for the Different Ligands[a]

	λ_{abs} free ligand	λ_{abs} Eu^{3+} complex	λ_{exc}	T
S_1	288 (34 722)	307 (32 573)	294 (34 014)	447 (22 371)
S_2	302 (33 113)	322 (31 056)	310 (32 258)	464 (21 552)
S_3	292 (34 247)	323 (30 960)	305 (32 787)	467 (21 413)
S_4	322 (31 056)	376 (26 596)	336 (29 762)	480 (20 833)
O_1	292 (34 247)	310 (32 258)	292 (34 247)	446 (22 422)
O_2	302 (33 113)			455 (21 978)
O_3	290 (34 483)	328 (30 488)	308 (32 468)	463 (21 598)
O_4	310 (32 258)	340 (29 412)	330 (30 303)	541 (18 484)

[a] In nanometers; values in parentheses are in inverse centimeters.

λ_{abs} values relative to the Eu^{3+} complexes, the shift to longer wavelengths observed for S_2/S_3 ligands is consistent with the more ionic character of the C═O bond, thus increasing mutual conjugation of pyridine and carboxamide groups.

The excitation spectra were recorded by monitoring the $^5D_0 \rightarrow {}^7F_2$ transition at 617 nm and were corrected from the spectral repartition of Xe lamp. The spectra are dominated by a broad excitation band (BEB), which is assigned to the absorption of the ligands. Table 3 shows the corresponding excitation maxima for all samples at 15 K. Transitions at 395 and 468 nm were observed and were attributed to the Eu^{3+} $4f^6$ intrashell $^7F_0 \rightarrow {}^5L_6$ and $^7F_0 \rightarrow {}^5D_2$ transitions, respectively. These transitions are always weak compared to those relative to the organic ligand and are even sometimes overlapped by BEB, which proves that luminescence sensitization via excitation of the ligands is much more efficient than the direct excitation of the own Eu^{3+} absorption levels. As illustrated in Figure 2, the excitation maxima are observed to vary in a manner similar to the position of the absorption edges.

Emission spectra of Gd^{3+} samples were recorded at 15 K under UV excitation (290 nm). All of the spectra exhibited a broad phosphorescence band that corresponds to the emission from the triplet state of the ligands.[36] The triplet state energy levels (T) were taken at the maximum of emission and are reported in Table 3. The same red shift as above was observed for T values as $T(O_1-S_1) > T(O_2-S_2) > T(O_3-S_3) > T(O_4-S_4)$.

Except for S_4, no significant difference in either the absorption/excitation levels or the triplet state levels was noticed between the silylated ligands and the organic ones. This is once more consistent with the fact that chelate structures are not affected by the silica network.

Eu^{3+} Emission Properties. The luminescence behavior of the EuS_j and EuO_j ($j = 1-4$) samples has been investigated at 15 K by direct excitation of the ligand (337.1 nm). Representative emission spectra are given in Figure 3 for the EuS_3 and EuO_3 systems. The optical transitions result from relaxation from the first $^5D_0$ excited state of Eu^{3+} to the first five levels of the ^7F_J ($J = 0-4$) ground state. The $^5D_0 \rightarrow {}^7F_2$ emission around 616.0 nm is the most predominant transition, which agrees with the amorphous character of the hybrid samples. As shown in Table 4, only minor differences were seen in the spectral repartition of the various

(30) Renaud, F.; Piguet, C.; Bernardinelli, G.; Bünzli, J. C. G.; Hopfgartner, G. *Chem. Eur. J.* **1997**, *3* (10), 1660.
(31) Sabbatini, N.; Guardigli, M.; Mecati, A.; Balzani, V.; Ungaro, R.; Ghidini, E.; Casnah, A.; Pochini, A. *Chem. Commun.* **1990**, 878.
(32) Galaup, C.; Picard, C.; Cazaux, L.; Tisnès, P.; Aspe, D.; Autiero, H. *New J. Chem.* **1996**, *20* (10), 997.
(33) Crosby, G. A.; Whan, R. E.; Alire, R. E. *J. Chem. Phys.* **1961**, *34* (3), 743.
(34) Malta, O. L. *J. Lumin.* **1997**, *71*, 229.
(35) Malta, O. L. *Spectrochim. Acta, Part A* **1998**, *54*, 1593.
(36) Prodi, L.; Maestri, M.; Ziessel, R.; Balzani, V. *Inorg. Chem.* **1991**, *30*, 3798.

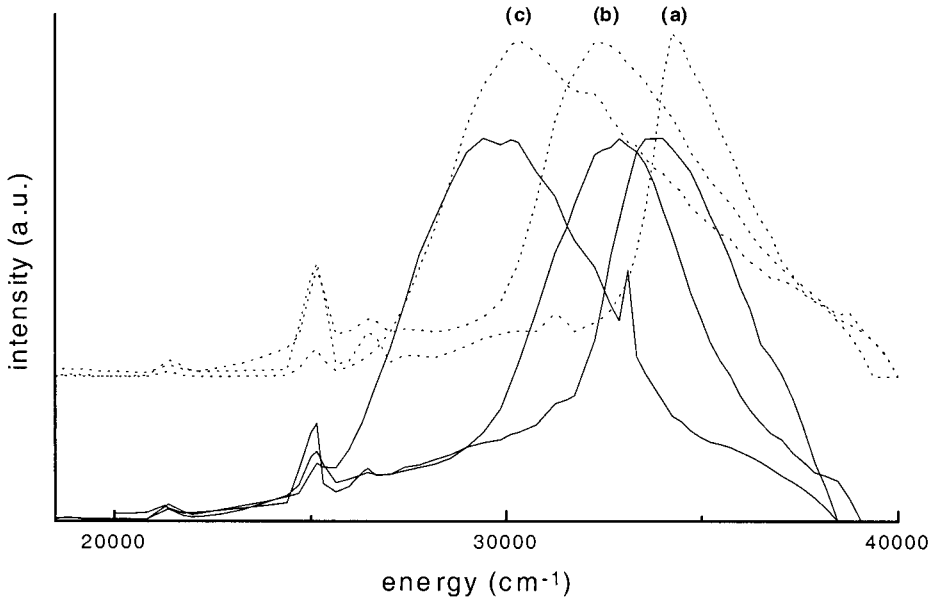

Figure 2. Excitation spectra of EuS_1/EuO_1 (a), EuS_3/EuO_3 (b), and EuS_4/EuO_4 (c) complexes. Black lines are related to hybrid complexes, and dot lines are related to organic complexes.

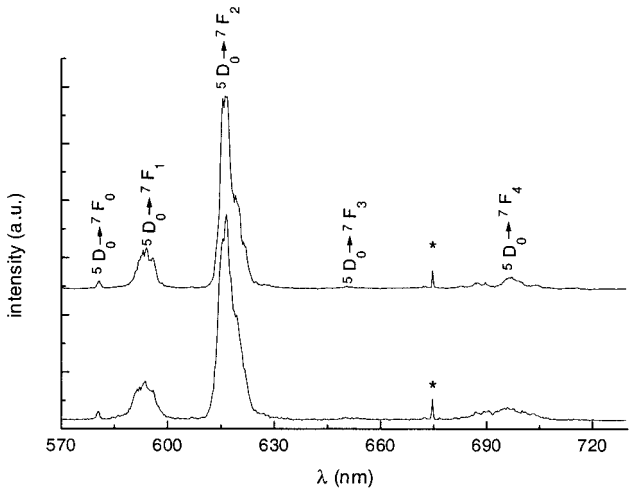

Figure 3. Emission spectra of EuO_3 (upper curve) and EuS_3 (bottom curve) in the 570−730 nm range (λ_{exc} = 337.1 nm, T = 15 K, delay = 75 μs). * corresponds to 2nd-order-scattered laser beam.

Table 4. $^5D_0 \rightarrow {}^7F_2/{}^5D_0 \rightarrow {}^7F_1$ Relative Intensities (I), Maximum (λ_{max}), Half-width ($\Delta_{1/2}$), and Lifetime (τ) of the $^5D_0 \rightarrow {}^7F_2$ Transition for the Eu^{3+} Complexes[a]

	I	λ_{max}	$\Delta_{1/2}$	τ
S_1	5.21	616.4	150	0.94
S_2	5.03	616.2	166	0.70
S_3	5.32	616.2	130	0.86
S_4	5.14	616.2	104	1.02
O_1	4.35	616.0	107	1.06
O_2				
O_3	4.90	616.2	96	1.35
O_4	4.83	617.0	68	1.20

[a] λ_{max} is in nanometers, $\Delta_{1/2}$ is in inverse centimeters, and τ is in milliseconds.

compounds when excited at 337.1 nm with respect to the positions and relative intensities of emission bands. This shows that the Eu^{3+} local environment is not mainly affected by changing the substituents on the amide functions or by grafting the ligand to the silica network. All of the $^5D_0 \rightarrow {}^7F_J$ luminescence decays fit a single-exponential law, confirming that all Eu^{3+} ions lie in the same average environment. The resulting lifetimes (see Table 4) are on the same order of magnitude for all samples. Nevertheless, it appears as a general trend that the lifetimes in hybrid materials are slightly lower than those in the corresponding organic complexes. This can be ascribed to a possible quenching by OH or silanol groups. The EuS_3 lifetime is particularly lowered, which is due to a higher concentration of residual hydroxyls in relation to the starting S_3 ligand structure (see Scheme 2). This effect remains however limited, confirming that the ligands used are efficiently shielding Eu^{3+} ions from their surroundings. In the case of EuS_2, the lowering of the $^5D_0$:Eu lifetime can be correlated with the broadening of the $^5D_0 \rightarrow {}^7F_2$ emission transition, which probably indicates an intense coupling of the electronic states with the OH vibrations. This is illustrated in Table 4 where the evolution of the half-width of the $^5D_0 \rightarrow {}^7F_2$ transition is reported. A multiplicity of inequivalent bonding sites are present in an amorphous host such as silica. Even if organic molecules shield Eu^{3+} ions from their environment, this inhomogeneous distribution of sites can be sensitive in hybrid materials insofar as OH groups of the siloxane matrix can participate to the second coordination sphere or can create hydrogen bondings with the chelating groups. These modifications will induce a broadening of the emission peaks, whereas their influence on spectral repartition and on luminescence lifetimes, for which the role of the first coordination sphere is predominant, are more limited. The emission intensity relative to hybrid materials was found to increase in this order: $EuS_1 < EuS_3 \leq EuS_2 < EuS_4$. This behavior is directly related to the capability of the ligands for absorbing and transferring energy to the Eu^{3+} ions. EuS_4 clearly exhibits improved optical characteristics resulting from enhancement of absorption efficiency due to a more conjugated system. The increased luminescence efficiency for EuS_2 and EuS_3 as compared with EuS_1 is probably related to the substitution of N−H bonds by N−C bonds, thus reducing possible nonradiative mechanisms via N−H vibrations.[25−27] Other factors

such as the triplet state level[37,38] can however not be excluded.

In the studied systems, few differences are observed in the luminescence properties between the organic complexes and the derived hybrid materials, showing that the silica network does not affect notably the optical characteristics of the organic part when both components are covalently grafted. In this study, it has been shown that minor differences in the chelate structure are likely to modify the luminescence relative quantum yields. As the method of synthesis can be easily applied to other ligands and to different modified alkoxysilanes, the desired properties can be tailored by an appropriate choice of the precursors. This way, we might expect to obtain stable and efficient hybrid phosphors. The influence of the silica network on the luminescence properties in such materials however needs further fundamental investigations.

CM9904739

(37) Sager, W. F.; Filipescu, N.; Serafin, F. A. *J. Phys. Chem.* **1965**, *69* (4), 1092.
(38) Latva, M.; Takalo, H.; Mukkala, V. M.; Matachescu, C.; Rodriguez-Ubis, J. C.; Kankare, J. *J. Lumin.* **1997**, *75*, 149.